Engineering Science and Technology, an International Journal 38 (2023) 101337

HOSTED BY

Contents lists available at ScienceDirect

Engineering Science and Technology, an International Journal

journal homepage: www.elsevier.com/locate/jestch

# An experimental study on the ballistic performance of ultra-high hardness armor steel (Armox 600T) against 7.62 mm × 51 M61 AP projectile in the multi-hit condition

Engin Göde [a,*], Atanur Teoman [b], Barış Çetin [c], Kürşat Tonbul [d], Kemal Davut [e], Melih Cemal Kuşhan [f]

[a] STM Savunma Teknolojileri Mühendislik ve Ticaret A.Ş., Ankara 06530, Turkey
[b] Defense Technologies Research Group, Eskişehir Osmangazi University, Eskisehir 26040, Turkey
[c] FNSS Savunma Sistemleri A.Ş., R&D Center, Ankara 06830, Turkey
[d] Presidency of the Republic of Türkiye, Defense Industry Agency, Ankara 06420, Turkey
[e] Department of Materials Science and Engineering, İzmir Institute of Technology, İzmir 35430, Turkey
[f] Department of Aeronautical Engineering, Eskişehir Osmangazi University, Eskisehir 26040, Turkey

ARTICLE INFO

*Article history:*
Received 15 August 2022
Revised 17 December 2022
Accepted 7 January 2023
Available online 19 January 2023

*Keywords:*
Ballistic resistance
Armox 600T
7.62 mm × 51 M61 AP projectile

ABSTRACT

In this study, Armox 600T armor steel was ballistically tested against 7.62 mm × 51 M61 AP projectile. The experimental design was constructed on the basis of the worst-case scenario which is the highest possible impact velocity in the multi-hit condition. The ballistic tests revealed that Armox 600T could defeat the worst-case scenario with a thickness of 12 mm. Furthermore, the damaged and undamaged regions were inspected microstructurally in a detail manner aiming to observe the possible fractographic modes of the studied material. Finally, high resolution optical scanning efforts were also added to the experimental work whose results uncovers the possible improvement areas regarding the quantification of the results of ballistic testing.


## 1. Introduction

Metallic materials are widely used in armor applications [1,2]. Although lower density metals are available for ballistic protection including composite structures and ceramics; mostly metallic materials (especially steel and aluminum) are the major constituent for various ballistic and structural applications [3]. In that sense, selection of the appropriate armor alternative is barely dependent on the ballistic resistance and the protection requirement of the specific design zone of the vehicle. Therefore, benchmark studies have been ongoing for decades aiming to achieve the optimum armor design whose outcome is to encounter many research focusing on the before mentioned comparison-based efforts [4–6]. From a general perspective, it could be stated that armor steels dominantly provide optimal ballistic protection against various threats with appropriate budgets [7]. At this point, it is worth to clarify that armor steels are mainly classified into three grades as (i) rolled-homogeneous armor (RHA), (ii) high-hardness (HH) armor and (iii) ultra-high hardness (UHH) armor conforming to MIL-DTL-12560 [8], MIL-DTL-46100 [9] and MIL-DTL-32332 [10] standards, respectively. Ballistic performance of RHA was developed importantly with the increase in hardness by U.S. Army Research Laboratory (ARL) in the early 1990's. RHA with hardness from 241 to 388 Brinell (BHN) and HH with hardness from 477 to 534 BHN (maximum thickness of 50.8 mm) are two armor steel grades used in combat vehicles of US army for the hull design [11]. On the contrary, UHH steels are widely used in appliqué and structural armor applications due to improved ballistic resistance provided by huge hardness which in particular enables to damage the projectile, at least smoothen its sharp edge [12]. Recently, there were also some attempts to develop and commercialize dual hardness armor (DHA) steels, but due to the manufacturing difficulties and technical constraints, they have been mostly replaced by monolithic alternatives consisting of UHH grades with a hardness of 600 BHN or greater [3]. Since there is not a totally linear correlation between the hardness and the ballistic resistance of the armor steel, designing of armor steel as a functionally graded approach may offer high potential if the mentioned problems related to manufacturing route can be eliminated. In this regard, it should be taken into account that target material hardness is an important parameter on the penetration but not the only variable [13]. Particularly, the strain hardening rate, fracture

* Corresponding author.
*E-mail address:* engingode81@yahoo.com (E. Göde).
Peer review under responsibility of Karabuk University.

https://doi.org/10.1016/j.jestch.2023.101337
2215-0986/

behavior and phase transformation during the deformation (if any) also contribute to ballistic performance which makes the process more difficult and unpredictable [4,14–17]. In the previous study of Showalter et al. (2007) [18], it was observed that ballistic performance improved with increase in hardness up to nearly 400 BHN level of steel plate and against AP projectiles. For higher hardness than 400 BHN, ballistic performance showed a horizontal course against 7.62 mm APM2 and reduced against 12.7 mm APM2 projectiles, indeed. This result reveals that the ballistic resistance is influenced not only by the hardness and toughness of the armor steel but also the kinetic energy level of the projectile. This is actually a well-known fact as explicitly displayed in the Milne-de-Marre graph (Fig. 1).

Increasing the kinetic energy level and/or altering the hardness of the armor steel definitely lead to unique results regarding fracture mechanics either. For instance; the relationship between ballistic performance and the fracture modes are not the same for RHA, HH and UHSS grades. Fig. 2 provides and overall picture regarding the general relationship between the specific armor steel grades and fractographic tendencies. For the case of RHA, plastic flow is effective on performance and ductile hole formation occurs in the steel damage mechanism (Mode A). Increasing the hardness of the armor steel triggers the formation of adiabatic shear bands (ASB) which are generally followed by soft plugging. Ballistic performance could be reduced to some extent when plugging occurs in armor steels (Mode B). The probable reason is the premature failure due to formation of ASB. For UHS grades, an AP projectile is often shattered by means of the huge hardness of the armor steel. In this defeat mechanism, armor steels possess a brittle fracture mode which mostly consists of quick formation and accelerated propagation of micro-cracks.

It is quite crucial to better understand the relation among the hardness, ballistic resistance and fractographic behavior of the armor steels by taking into account the macro-mechanical and micro-structural phenomena. In this view, there exist numerous research studies [3,11,18,21–23] dedicated to the indicated scientific area. Cimpoeru, 2016 [7] discussed the relationship between mechanical properties of armor steels and ballistic performance. Similarly, Gooch et al. (2004) [11] conducted miscellaneous ballistic tests to Armox armor steels to compare the ballistic limit velocities regarding existing test data. In the research of Gooch 2004 et al. [11], Armox 600T steel with thickness of 15.2 mm was determined to provide quite better mass efficiency (i.e., areal density) compared to other armor steel grades as a superior appliqué armor steel. Showalter et al. (2007) [18] also examined the ballistic performance of UHH steels (Armox 600T and Armox Advance) in terms of military specification requirements [3]. Likewise, Rapacki et al. (1995) [24] conducted a study on ballistic performance of Armox 600T. However; there is not any existing study which is specifically devoted to unveil the ballistic performance of Armox 600T steel against AP projectile together with fractographic exam-

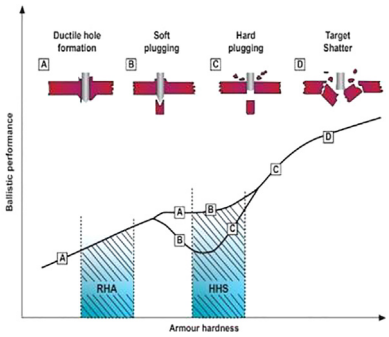


**Fig. 2.** Fractographic tendencies (re-created after [4]).

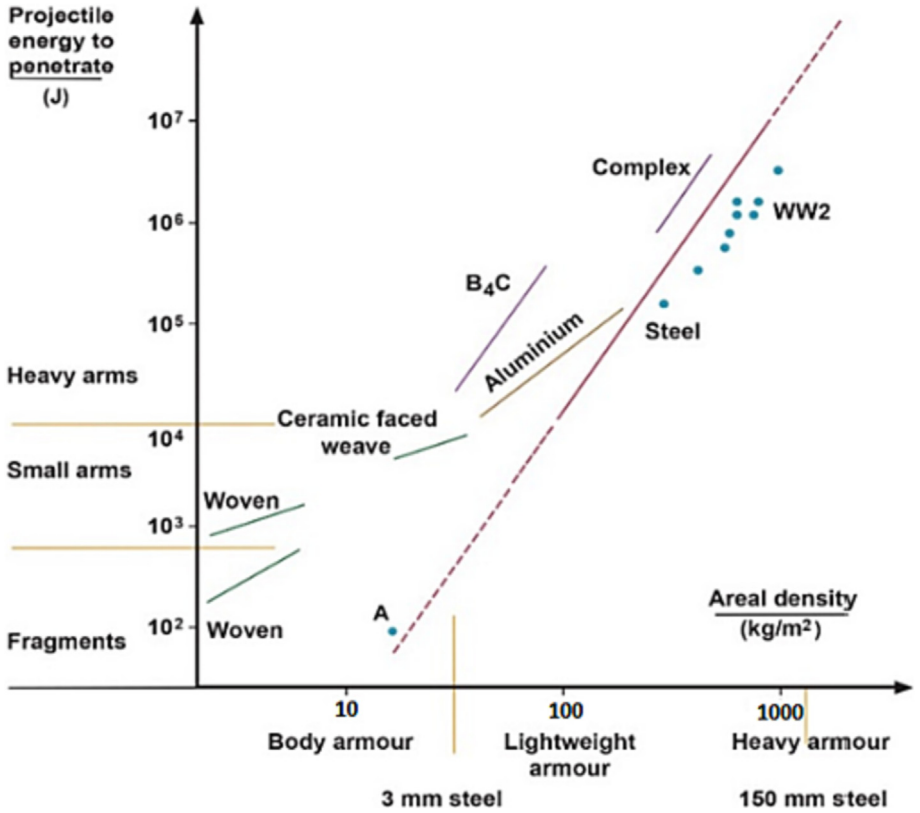


**Fig. 1.** Milne-de-Marre graph showing projectile energy to penetrate as a function of density (re-created after [19,20]).

ination including microstructure and texture analysis. This study aims at closing the gap by conducting ballistic tests in out-door polygon. Furthermore; damaged and undamaged surfaces were both examined with optical and scanning electron microscopes (SEM) and also with the electron back-scatter diffraction (EBSD) technique aiming to uncover the micromechanical motivations of the fracture modes. Lastly, in order to provide more quantitative data from ballistic tests, the damaged armor steel plates were 3D laser scanned with high resolution to obtain the crater topology data.

## 2. Materials and methods

### 2.1. Target material

In this study, basically the ballistic performance of Armox 600T (which is a member of UHH armor steel family) was investigated. The dimensions of the target plate are 200x200 mm and has a thickness of 12.4 mm. The figure in the product designation is the approximate hardness value as Brinell grades. Armox 600T steel is a commercialized product of Swedish Steel Oxelösund AB (SSAB) company and it is in service for defense industry applications for over two decades [25,26]. In general, Armox 600T has a nominal hardness of 570–640 HBW and a min. impact energy of 12 J at −40 $^{0}$C and mechanical properties of Armox 600T are presented in Table 1. The nominal chemical composition of Armox 600T is also given in Table 2.

### 2.2. Projectile

Ballistic tests were performed with the 7.62 mm × 51 M61 AP projectiles which are shown schematically in Fig. 3.

The steel core and the construction of 7.62 mm M61 AP projectile used for armor system ballistic test are shown in Fig. 4 and Fig. 5 and properties of this projectile which were extracted from the open-source literature data is given Table 3.

### 2.3. Ballistic test set-up

Armox 600T steel plate was installed to a specific fixture with secured armor panel (Fig. 6). Then, ballistic tests were performed for the armor plate. The fixture holding the armor panel was heavy enough to perform ballistic tests. There are clamps providing equal holding force for the armor panel. Target was secured by bolts located on the clamps. A chronograph which measures projectile impact velocity was installed next to the target. Steyr SSG 08 sniper rifle was used for shootings.

### 2.4. High resolution optical scanning set-up

To perform 3D scanning operations, a specifically designed optical system was used at Psaron HTI Company. In particular, PSARON 3D Laser scanner which runs with a laser source with 632 nm wavelength was employed to measure the surface profile of ballistically tested armor plate. The system basically composed of a laser source, a detector and a CMOS camera. The diffracted signals of the laser source were processed through certain signal processing algorithms which in turn yields the topological data of the surface at which the laser interferes. By means of this optical set-up, a scanning resolution of 15 μm is assured in both lateral and axial direction. The system can provide one-dimensional depth profiles at any cross-sections. The orientation of the laser source is adjusted so that the full texture of steep gradients was fully resolved. The picture of the optical scanning set-up is depicted in Fig. 7. Moreover, a real-time high magnification image that was taken from CMOS camera is given in Fig. 8.

### 2.5. Micro-structural analysis

The microstructure of the cross-sections of the steel plates, including partially penetrated regions after the ballistic tests were examined. For this metallographic examination, the specimens were sectioned by electrical discharge machining (EDM) and also by using an abrasive cut-off machine. Afterwards, the specimens were grinded with 320 and 500 grit ANSI SiC papers and then polished with 9 μm, 3 μm and 1 μm diamond paste. Lastly, specimens were etched with picral (4 g picric acid, 100 mL ethanol) solution. Nikon LV-150 N optical microscope was used to take optical micrographs of the specimens at ×50–×500 magnification under bright field illumination. The front face of partially penetrated regions and cross sections of the specimens were also examined under FEI 430 scanning electron microscope (SEM) using 20 kV accelerating voltage and secondary electron detector. Lastly, EBSD technique was employed to reveal additional microstructural details. For EBSD analysis Zeiss Merlin field emission gun (FEG) scanning electron microscope equipped with EDAX/TSL EBSD system and Hikari EBSD camera was used. The accelerating voltage was 15 kV, beam current 6nA and the working distance 12 mm, EBSD maps of 54 × 54 μm were measured on a hexagonal grid with a step size of 50 nm.

## 3. Result and discussion

### 3.1. Ballistic test

Ballistic test was performed against 7.62 mm × 51 M61 AP projectile for Armox 600T armor steel plate. Eight shootings were performed in the ballistic test up and the ballistic test results were shown in Table 4. After test views for the armor and projectile pieces were also seen in Fig. 9.

As seen in Fig. 9, shootings were defeated by the armor steel. These UHH steels typically showed shattered projectile cores compatible with the existing studies [14]. The studied material with the thickness of 12 mm is capable of eliminating 7.62 mm × 51 M61 AP projectile threat in multi-hit regime. More particularly, the projectiles with 815–829 m/s impact velocities could be defeated. 7.62 mm × 51 M61 AP (hard steel core) ammunition or its equivalent is a defined threat in international ballistic standards such as VPAM-APR 2006 [31] CSN EN1522 [32] and CSN EN 1523 [33]. The impact velocity of this ammunition on the target is defined as 820 ± 10 m/s in these ballistic standards. It is seen that the impact velocities of the ammunition within the scope of this study are appropriate.

**Table 1**
Chemical composition of Armox 600T (% wt) [27].

| C* (Max %) | Si* (Max %) | Mn* (Max %) | P (Max %) | S (Max %) | Cr* (Max %) | Ni* (Max %) | Mo* (Max %) | B* (Max %) |
|---|---|---|---|---|---|---|---|---|
| 0.47 | 0.7 | 1.0 | 0.010 | 0.003 | 1.5 | 3 | 0.7 | 0.005 |

*Intentional alloying elements.

**Table 2**
Mechanical properties of Armox 600T [3].

| Hardness (BHN) | Charpy-V -40 °C 10 × 10 mm (J) | 0.2 % Yield Strength (N/mm$^2$) | Tensile Strength (N/mm$^2$) | Elongation (%) |
|---|---|---|---|---|
| 570–640 | Minimum 12 | 1500[a] | 2000[a] | 7[a] |

[a] Typical values.

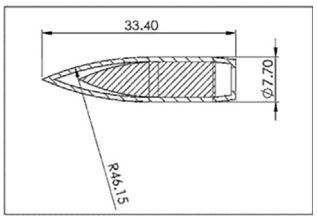


**Fig. 3.** Schematic diagram of the 7.62 mm × 51 M61 AP projectile [28].

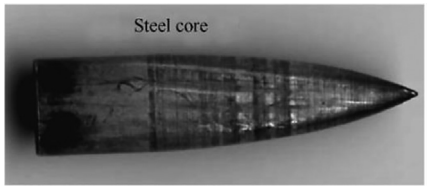


**Fig. 4.** Steel core 7.62 mm × 51 AP M61 AP projectile [29].

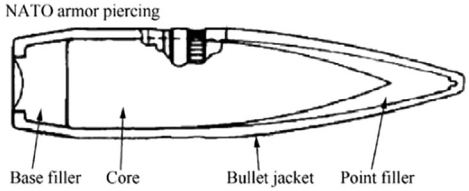


**Fig. 5.** Schematic structure of a 7.62 mm 51 mm M61 AP projectile [29].

**Table 3**
Properties of 7.62 mm × 51 M61 AP projectile [29,30].

| Ammunition | Length (mm) | Weight (g) | Diameter (mm) | Muzzle Velocity (m/s) | Nose Performance Coefficient ($\bar{N}$) |
|---|---|---|---|---|---|
| Cartridge | 71.1 | 25 | | | |
| Projectile | | 9.55 | 7.82 | 838 | 1.39 |
| Steel core | | 3.7 | 6.06 | | |

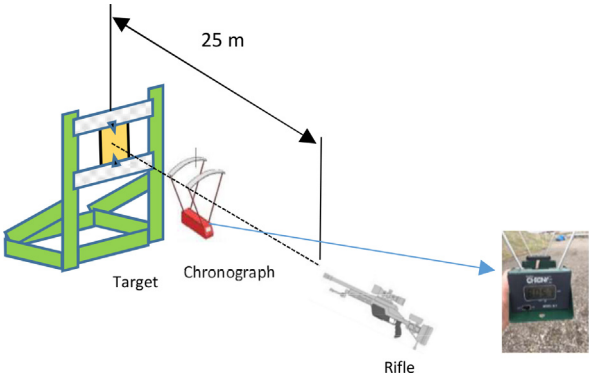


**Fig. 6.** Standalone armor test system.

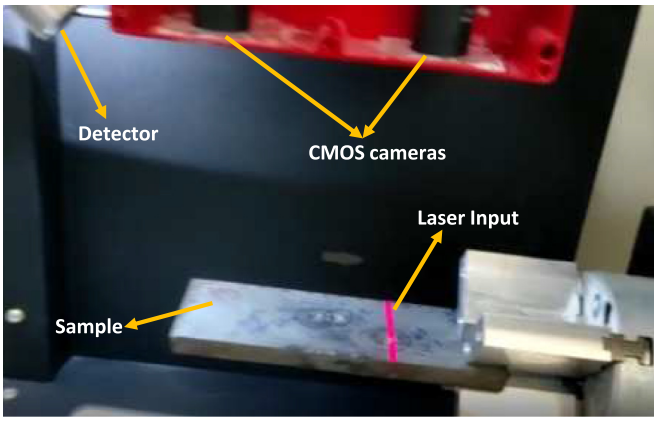


**Fig. 7.** 3D optical scanning set-up.

Various investigations were made to observe the changes in the microstructure of the material after the ballistic test. In this context, two major actions were taken within the scope of this study. Firstly, ballistically tested material was investigated via deep microstructural examinations including SEM and EBSD analysis and moreover any distinguishing character regions to obtain valuable data regarding the fracture modes. Secondly, the crater topology was searched in a detailed manner with optical scanning approach aiming to collect any possible data related to the plastic deformation/damage that the material exhibit. This quantitative data is capable of bringing out crucial clues in material characterization and/or possible technical alternatives to improving the ballistic performance of the same grade armor steels.

### *3.2. Microstructural and fractograhic analysis*

The microstructure and fracture surfaces and the specimens after ballistic test are shown in Fig. 10. The fracture surfaces, shown in Fig. 10.a, c and f show no signs of deformation but only cracking. The microstructure of the unaffected region is composed of mainly tempered martensite (Fig. 10d). Because of the harder martensitic structure and extremely high deformation rates caused by the shootings, the material cannot plastically deform, but instead crack. The cracks are visible at the fracture surfaces as well (Fig. 10c and d). Those cracks extend through the thickness below the indentation (Fig. 10a). The optical micrograph of a crack penetrating through the thickness of the specimen after ballistic test is shown in Fig. 10a. Here, secondary cracks propagating in lateral direction are also visible. Higher magnification observation of these cracks in Fig. 10.f reveal that cracks extend through prior austenite grain boundaries (PAGB). Segregation of impurity elements and carbide precipitation during austenitization and tempering can cause weakening of prior austenite grain boundaries [34]. Upon high strain rate loading, those weakened boundaries would then cause formation of cracks. It should also be noted that, no significant relation between cracks and plate or lath boundaries were found.

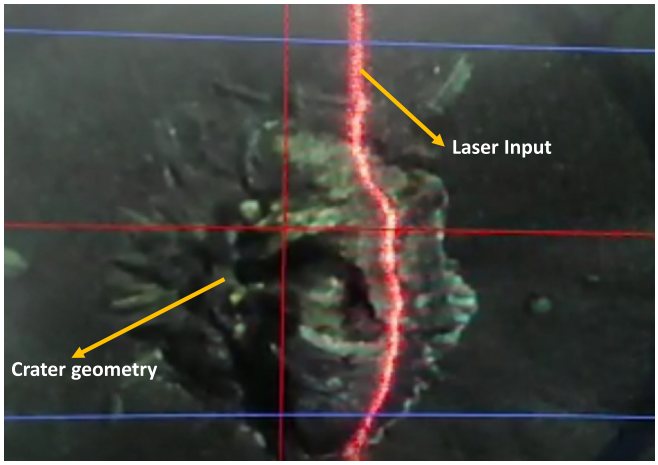


**Fig. 8.** High magnification image taken from CMOS camera during scanning.

**Table 4**
Ballistic test results for Armox 600T armor steel.

| Shooting number | Impact velocity (m/s) | Result | Remarks |
|---|---|---|---|
| 1 | 829 | Partial Penetration | without marks |
| 2 | 827 | Partial Penetration | without marks |
| 3 | 815 | Partial Penetration | without marks |
| 4 | 825 | Partial Penetration | without marks |
| 5 | 823 | Partial Penetration | without marks |
| 6 | 817 | Partial Penetration | without marks |
| 7 | 828 | Partial Penetration | without marks |
| 8 | 822 | Partial Penetration | bulge without cracks |

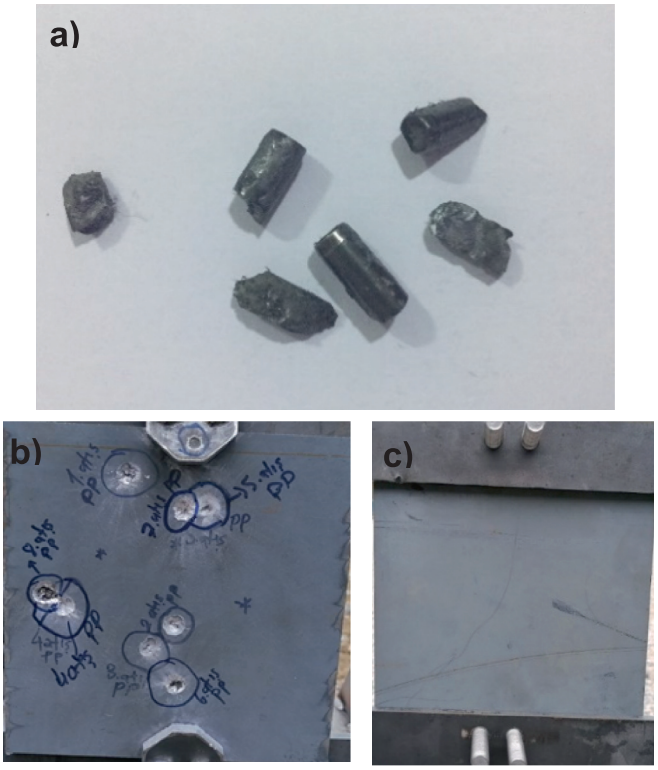


**Fig. 9.** a) Projectile pieces, b) front face and c) back face of Armox 600T armor steel after ballistic test.

Johnson-Cook damage model or its numerous derivatives basically rely on the fact that the hydrostatic stress (which means high stress triaxiality factor) hastens the fracture of the materials by triggering the void growth rate. For this type of model, void growth rate is independent of the orientation of the nucleating voids, indeed. However; during crack propagation type failure modes with high velocity impact loads as in the case of the current study,

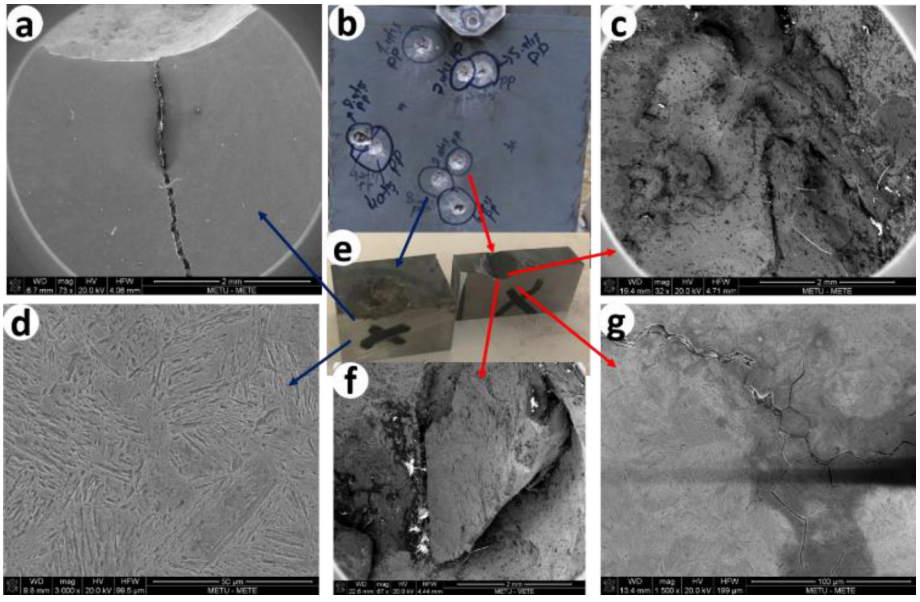


**Fig. 10.** a) Cross section under the indentation of partially penetrated shooting #2, b) overview of the shootings on the steel plate, c) fracture surface caused by shooting #3, d) microstructure of the cross-section of an unaffected region, e) cross-sections #2 and #3 prepared for microstructural examination, f) fracture surface caused by shooting #2, g) microstructural of cross-section under the shooting #2 (PAGB: prior austenite grain boundary).

advanced damage models are engaged. In general, those are taking into account physcial phenomena such as confinement pressure, crack interaction and etc. [35,36].

A region of the same armor plate, away from indentations was also examined via optical microscope (Fig. 11b) and EBSD technique (Fig. 12). The EBSD pattern quality map (Fig. 12a) also shows that the structure is mainly composed of tempered martensite. Trace amount of pro-eutectoid ferrite is also present. Those ferrite regions have two distinct morphologies, i) polygonal ferrite (equiaxed grains) and ii) acicular ferrite showing Widmanstaetten morphology. Ferrite forms with the acicular morphology, when cooling rates are high (i.e. quenching) which limits diffusion. The inverse pole figure map (Fig. 12.b) reveals prior austenite structure since martensite needles and plates formed from same parent austenite have the same orientation due to variant selection mechanism. The kernel average misorientation (KAM) map shown in Fig. 12.c shows higher misorientations in the martensitic regions due to higher dislocation density associated with the shear mechanism involved in the formation of martensite. The ferritic regions exhibit very low KAM values since they are formed via diffusion mechanism. The grain orientation spread (GOS) map (Fig. 12.d) shows results similar to KAM map. The KAM distributions shown in Fig. 13.a exhibit bi-modal distribution. Due to higher defect density, martensitic regions exhibit highest possible KAM values around 5 degree. On the other hand, polygonal and acicular ferritic regions exhibit KAM values lower than 1 degree. It should be noted that, during EBSD measurements both ferrite and martensite regions are indexed as BCC. Due to the effect of tempering, that reduces defect density some regions exhibit intermediate KAM values. Fig. 13.b shows the distribution of geometrically necessary dislocations. Since the microstructure is mainly composed of martensite, the dislocation density distribution is piled up to higher values.

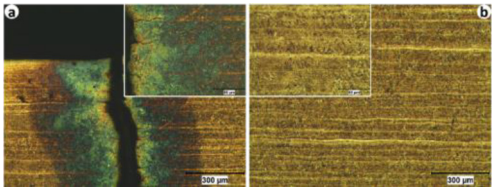


**Fig. 11.** Optical micrographs taken at 50x (and insets taken at 200x) magnification showing: a) cross section under the indentation of the partially penetrated shooting 2#, b) a region far from the indentation.

The grain size distribution of martensite-ferrite regions is given in Fig. 14.a. Large fraction of grains have a size smaller than 1 µm, since majority of the structure is martensitic. Acicular and particularly polygonal ferrite grains' size are larger than 1 µm. The average size of retained austenite grains is around 0.1 µm. In this sample the retained austenite fraction is less than 1 %, and retained austenite grains are actually untransformed regions left between martensite plates and needles. Nevertheless, since its fraction is very low, the influence of retained austenite on overall mechanical properties is low as well.

The microstructure analysis results show presence of trace amount of ferrite. Armor plate steels ideally should contain

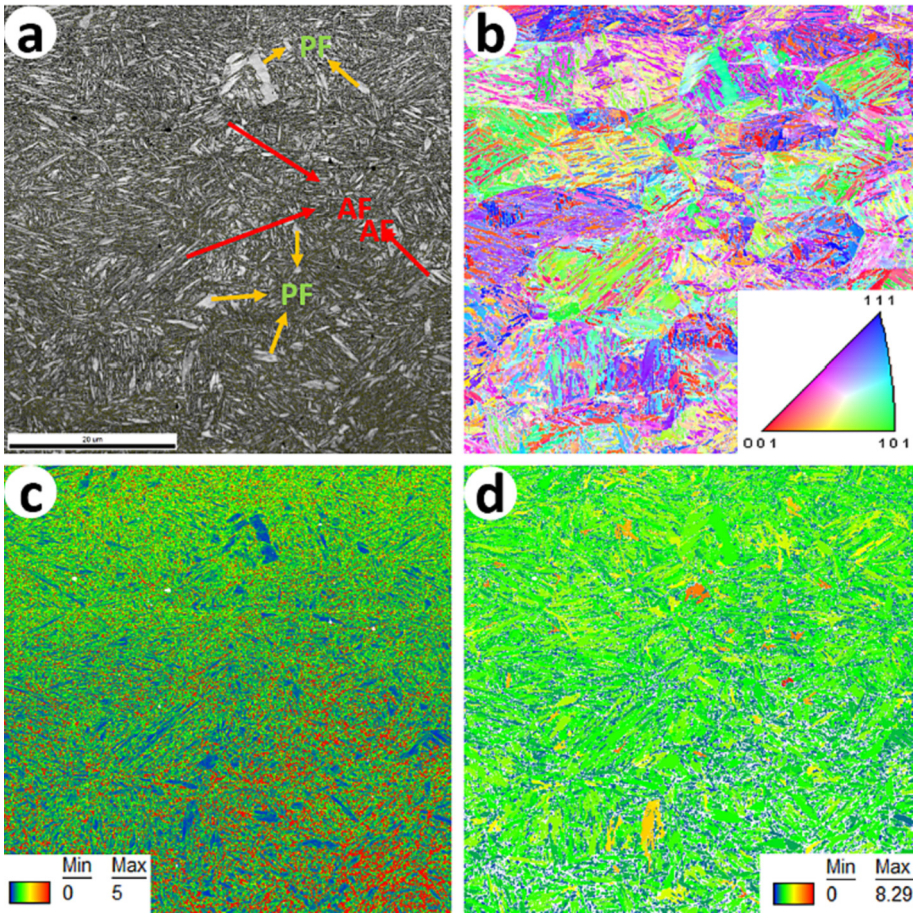


**Fig. 12.** EBSD results of a region far from indentations: a) pattern quality map with high angle (>15$^0$) grain boundaries (PF: polygonal ferrite, AC: acicular ferrrite), b) inverse pole figure (IPF) map w.r.t. normal direction, c) Kernel average misorientation (KAM) map, d) grain orientation spread (GOS) map.

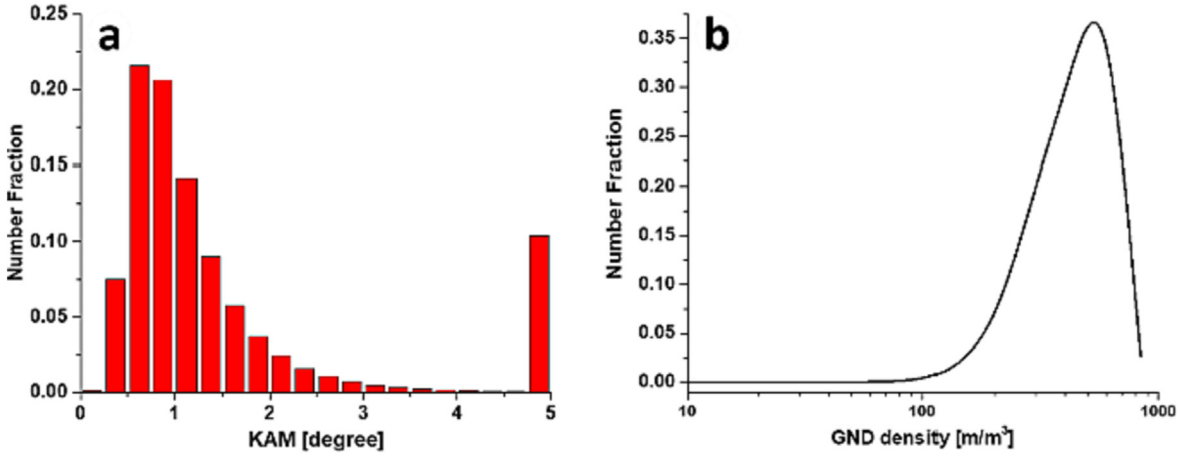


**Fig. 13.** a) KAM distribution and b) geometrically necessary dislocation density distributions of BCC-indexed regions.

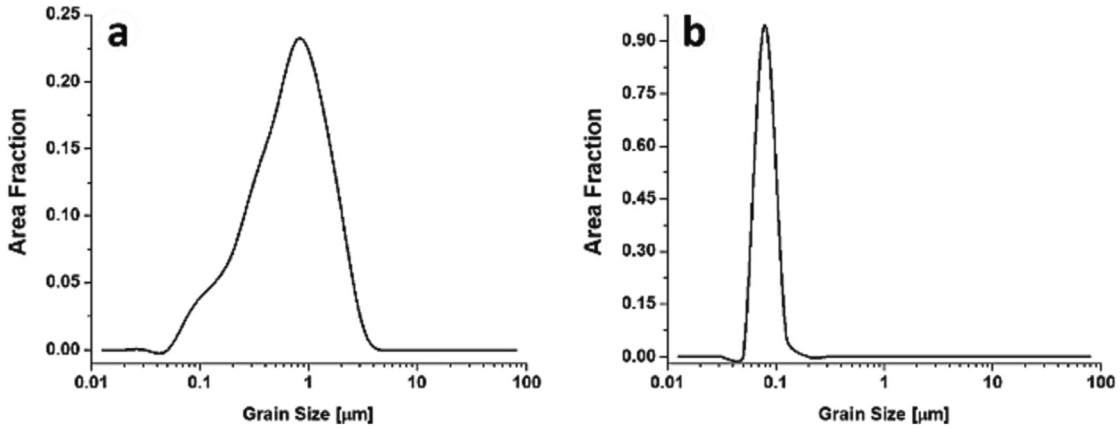


**Fig. 14.** Grain size distributions of: a) BCC-indexed regions and b) FCC-indexed regions.

100 % tempered martensite to obtain optimal combination of penetration resistance and impact toughness. Extremely fine structure of martensite contributes to this optimal combination of properties. Fine grained ferrite also has impact toughness values comparable to martensite. However, ferrite will lower the penetration resistance. For the present Armox 600T steel, trace amounts of ferrite ($\ll$4%) is observed usually at mid-thickness regions. Therefore, the influence of ferrite on impact toughness could considered negligible.

The hardness distribution along the thickness of the armor plate is given in Fig. 15. The average hardness is 635 BHN and standard deviation is 20.5 BHN. Those hardness values are typical for martensitic structures. It should also be noted that one side of the plate has slightly higher hardness values. The segregation of Mn during continuous casting to one side, differences in cooling rate during quenching can cause this difference. Nevertheless, the difference is less than 10 % of the average hardness and both sides of the plate have higher hardness values within specifications.

### 3.3. 3D optical scanning analysis

By using of 3D optical scanning, 3D topology data was created and shown in Fig. 16.a. Those 3D data can then be used to obtain 1D depth profile in any desires cross-section as can be seen in Fig. 16.b. This profilometric data can be normalized as the ratio of the total thickness over max. crater depth after which may be used as a quantitative criterion in ballistic tests. Besides that, it is also possible to determine the volume of the crater topology which could also serve as another important figure in benchmarking studies of different armor steel alternatives. The scanning data of the crater in Fig. 16 yields a max depth of 2.57 mm, a surface area of 225.48 mm$^2$ and a volume of 82.87 mm$^3$. These scanning efforts

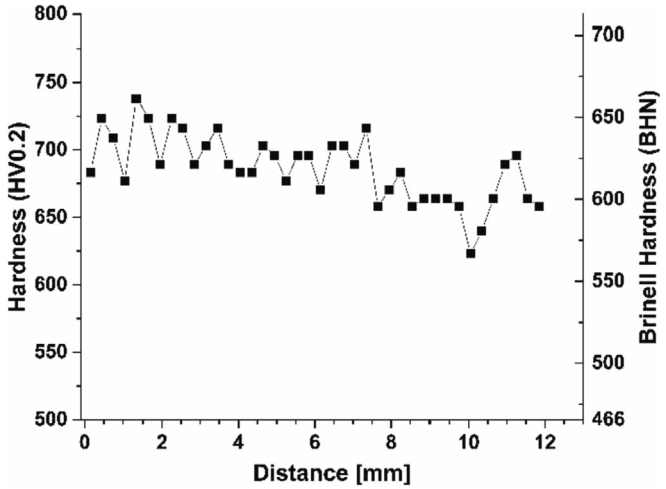


**Fig. 15.** Through the thickness hardness distribution of the armor steel.

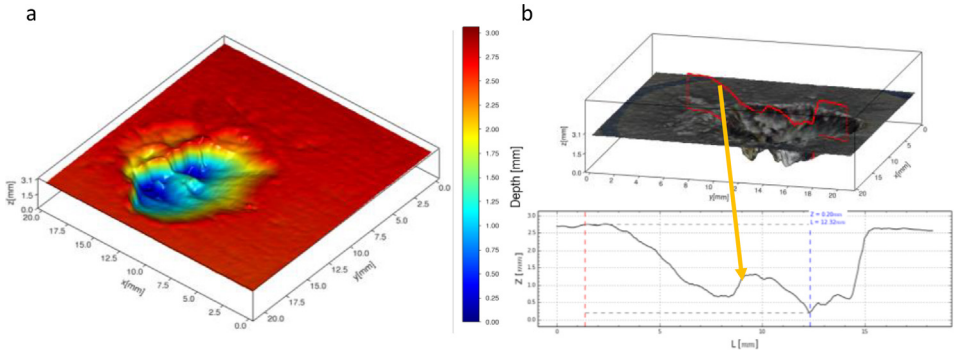


**Fig. 16.** a) 3D Topology data of the crater b) 1D profile depth of the specific cross-section (red line).

provide quantitative results out of ballistic test as intended. In our view, this emerging approach may open new opportunities for further scientific researches in terminal ballistic engineering field.

As an overall picture, it is observed that Armox 600T had a bulging type fracture behavior instead of localized conical damage which is an advantageous fact. The multi hit shootings did not influence the main ballistic resistance since the max depth of the craters is very similar.

## 4. Conclusion

Armox 600T armor steel was ballistically tested against 7.62 m m × 51 M61 AP projectile, which is the most commonly faces ballistic threat. In order to observe to worst case scenario, the tests were conducted in multi-hit condition. Aiming to unveil the fracture modes of Armox 600T, detailed microstructural observation was carried out for the damaged and undamaged regions. And finally, 3D optical scanning operations were employed to create quantitative data regarding the ballistic tests. The following conclusion can be drawn:

- 12 mm Armox 600T steel can eliminate 7.62 mm × 51 M61 AP projectile with velocities of 815–829 m/s in multi-hit condition.
- The major fractographic tendency of Armox 600T related to the designated ballistic threat, is prior cracking through thickness and followed by secondary cracking towards lateral direction. Therefore, ductile damage theory-based material models which absolutely foresee damage evolution through void nucleating and void coalescence as in the case of Johnson-Cook damage model, should not be used for the here presented material and case.
- The cracks were propagating in intergranular fashion, along the prior austenite grain boundaries, which deliver significant information concerning possible microstructural engineering-based solutions to improve the ballistic resistance.
- Armox 600T has almost completely tempered martensite microstructure, and less than 1 % retained austenite, which means that there is not any contribution related to TRIP (transformation induced plasticity) effect in its ballistic resistance. Due to fine martensitic structure, most of the grains are smaller than 1 μm, though some trace amounts of polygonal and acicular ferrite are also present. Through thickness hardness distributions were not homogeneous, nevertheless the hardness of both sides of the plate were within specifications.
- 3D optical scanning data can produce essential quantitative data, such as the maximum depth or the volume of the crater geometry. This new technique has great potential to quantitatively assess the ballistic performance of different armor steels.

## Declaration of Competing Interest

The authors declare that they have no known competing financial interests or personal relationships that could have appeared to influence the work reported in this paper.

## References

[1] M.L. Bekci, B.H. Canpolat, E. Usta, M.S. Güler, Ö.N. Cora, Ballistic performances of Ramor 500 and Ramor 550 armor steels at mono and bilayered plate configurations, Eng. Sci. Technol., an Int. J. 24 (4) (2021) 990–995.
[2] F.T.M. Van Wegen, E. Carton, New lightweight metals for armors, International Symposium on Ballistics, Florida, USA, 2011.
[3] D.D. Showalter, W.A. Gooch, M.S. Burkins, R.S. Koch, Ballistic testing of SSAB ultra-high hardness steel for armor applications, ARL-TR-4632 (2008).
[4] I.G. Crouch, Metallic armour from cast aluminium alloys to high strength steels, Mater. Forum. 12 (1988) 31–37.
[5] F.S.d. Luz, F.d.C. Garcia Filho, M.S. Oliveira, L.F.C. Nascimento, S.N. Monteiro, Composites with natural fibers and conventional materials applied in a hard armor: A comparison, Polymers 12 (9) (2020) 1920.
[6] R. Yadav, M. Naebe, X. Wang, B. Kandasubramanian, Body armour materials: from steel to contemporary biomimetic system, RSC Adv. 6 (2016) 116.
[7] S.J. Cimpoeru, The mechanical metallurgy of armour steels. Land Division Defence Science and Technology Group, DST-Group-TR-3305 (2016).
[8] MIL-DTL-12560K, Armor Plate, Steel, Wrought, Homogeneous (For Use in Combat-Vehicles and for Ammunition Testing), 2020.
[9] MIL-DTL-46100E, Armor Plate, Steel, Wrought, High-Hardness, 2009.
[10] MIL-DTL-32332A, Armor Plate, Steel, Wrought, Ultra-High-Hardness, 2018.
[11] W.A. Gooch, M.S. Burkins, R. Squillacioti, R.-M.S. Ros-Mari Stockman Koch, H. Oscarsson, C. Nash, Ballistic testing of Swedish steel Armox® plate for U.S. armor applications, in: 21st International Symposium on Ballistics Adelaide, South Australia. 2004.
[12] I. G. Crouch, S.J. Cimpoeru, H. Li, D. Shanmugam, Armour steels, in: Crouch, I.G. (Ed.), The Science of Armour Materials. Cambridge: Woodhead Publishing in Materials, (2017) pp. 60, 67-70.
[13] P. Frueh, A. Heine, K.E. Weber, M. Wickert, Effective depth-of-penetration range due to hardness variation for different lots of nominally identical target material, Def. Technol. 12 (2) (2016) 171–176.
[14] S.J. Manganello, K.H. Abbott, Metallurgical factors affecting the ballistic behavior of steel targets, J. Mater. 7 (2) (1972) 231–239.
[15] D.J. Papetti, in: Methods and Phenomena-Ballistic Materials and Penetration Mechanics, Elsevier, 1980, p. 145.
[16] R.L. Woodward, The interrelation of failure modes observed in the penetration of metallic targets, Int. J. Impact Eng. 2 (2) (1984) 121–129.
[17] Rawson, J.D.W., Dawson, D.I., 1972. Solidification technology. Proceedings of the First Army Materials Technology Conference, Portsmouth, New Hampshire, USA.
[18] D.D. Showalter, W.A. Gooch, M.S. Burkins, V. Thorn, S.J. Cimpoeru, R. Barnett, 2007. Ballistic testing of Australian Bisalloy steel for armor applications, in: 23rd International Symposium on Ballistics, Tarragona.
[19] A. Doig, Military Metallurgy, Maney Publishing, London, 1998.
[20] I.G. Crouch, The Science of Armour Materials. Woodhead Publishing in Materials, (2017) pp. 1-54, 117.
[21] Kaiser, H.J., Kern, A., Scharf, S., Gooch, W.A., 2011. Ballistic testing of Thyssenkrupp steel Europe armor steel in accordance with U.S. military armor specifications. 26th International Symposium on Ballistics, Miami, Florida, USA.
[22] S. Ryan, H.J., Li, M. Edgerton, D. Gallardy, S.J. Cimpoeru, Ballistic evaluation of an Australian ultra-high hardness steel. Faculty of Engineering and Information Sciences - Papers: Part B. 9.2016.

[23] J. Marcisz, W. Burian, J. Stępień, L. Starczewski, M. Wnuk, J. Janiszewsk, Static, dynamic and ballistic properties of bainite-austenite steel for armours, in: 28th International Symposium on Ballistics Atlanta, 2014, pp. 1348–1361.
[24] E. Rapacki, K. Frank, B. Leavy, M. Keele, J. Prifti, Armor steel hardness influence on kinetic energy penetration, in: Proceedings of the 15th International Symposium on Ballistics, Jerusalem, Israel.
[25] SSAB in brief. https://www.ssab.com/company/about-ssab/ssab-in-brief, Accessed on July 27th, 2022.
[26] SSAB. https://en.wikipedia.org/wiki/SSAB, Accessed on July 27th, 2022.
[27] Armox600T. Armox 600t general product decription. https://www.ssab.com/en/brands-and-products/armox/product-offer/armox-600t, Accessed on July 27th, 2022.
[28] A. Weiss, G.-B.-M. Stan Behavior of multi-layered metal plates under ballistic impact, in: Proceedings of 29th International Symposium on Ballistics, Edinburgh, Scotland, UK, 2016. 1925-1935
[29] M.G. Stewart, M.D. Netherton, Statistical variability and fragility assessment of ballistic perforation of steel plates for 7.62 mm AP ammunition, Def. Technol. 16 (3) (2020) 503–513.
[30] http://www.inetres.com/gp/military/infantry/rifle/762mm_ammo.html.
[31] VPAM-APR 2006, General basis for ballistic material, construction and product testing.
[32] CSN EN 1522, Windows, doors, shutters and blinds-Bullet resistance-Requirement and classification, 1998.
[33] CSN EN 1523, Windows, doors, shutters and blinds-Bullet resistance-Test method, 1998.
[34] F. Abe, New martensitic steels, in: A.D. Gianfrancesco (Ed.), Materials for Ultra-Supercritical and Advanced Ultra-Supercritical Power Plants, Woodhead Publishing, 2017, pp. 323–374.
[35] D.E. Grady, Shock-wave compression of brittle solids, Mech. Mater. 29 (3–4) (1998) 181–203.
[36] R. Zhang, B. Han, T.J. Lu, Confinement effects on compressive and ballistic performance of ceramics: a review, Int. Mater. Rev. 66 (5) (2021) 287–312.